Transmission of Subinertial Kelvin Waves through a Strait

THEODORE S. DURLAND AND BO QIU

Department of Oceanography, University of Hawaii at Manoa, Honolulu, Hawaii

(Manuscript received 9 July 2002, in final form 6 January 2003)

ABSTRACT

Solutions are found for the transmission of 1½-layer subinertial Kelvin waves through an ''ideal strait'' with parallel channel walls and square corner mouths. This is shown to be a wave interference problem similar to the classical optics problem of multiple beam interference. The outlet of an ideal strait has the same reflection characteristics as the inlet, setting up internal reflections within the strait and a consequent interference condition that has several important consequences: energy transmission of a strait is a function of channel length as well as width; transmission is frequency dependent, and approaches 100% at low frequencies for all channel widths, as long as the dynamics remain linear and inviscid; and the amplitude of the pressure signal on the downstream side of the channel approaches zero as the transmission approaches 100%. Numerical solutions are found for transmission through a strait with coastal geometry corresponding to the 200-m isobath at Lombok Strait, and the results show that the ideal strait model with an appropriate effective width can accurately predict the transmission characteristics of a more complex strait. In particular, even though the minimum channel width is less than one-fifth of the local Rossby radius, the strait is shown to approach total transmission within the intraseasonal frequency band.

1. Introduction

The question of whether and to what extent equatorial Indian Ocean processes impact the Indonesian Throughflow and the internal Indonesian seas has received considerable attention in recent years. The problem of how equatorial Kelvin waves reflect from the nonmeridional Indonesian coast continues to resist an analytical solution (D. W. Moore 2002, personal communication), but it is known that coastal Kelvin waves are generated in the process, bringing up another problem of both theoretical and practical interest: how do these coastal trapped waves interact with the relatively narrow straits that carry the Indonesian Throughflow? Arief and Murray (1996) first showed observational evidence that remotely generated Kelvin waves traveling down the coast of Indonesia might significantly modulate the branch of the Indonesian Throughflow (ITF) passing through the Lombok Strait, and Sprintall et al. (2000) presented convincing evidence that this does indeed occur. The question remains as to how much of the incident wave energy is transmitted through the Lombok Strait and how much can bridge the gap to continue down the coast and similarly affect subsequent channels. The Lombok Strait has minimum and average channel widths of about 0.2 and 0.4 times the local first mode baroclinic Rossby radius so that one might expect most of the incident energy to bypass the strait. In a 1½-layer model study, however, Qiu et al. (1999) showed virtually all of the Kelvin wave energy in the intraseasonal band (35–85 days) propagating through the Lombok Strait, raising the interesting question of how it is possible for the bulk of a Kelvin wave to squeeze through a strait with a width of only a fraction of a Rossby radius?

In this study we seek to answer the above question at the most basic level, and we retain the 1½-layer reduced-gravity dynamics. Although the southern mouth of Lombok Strait has a sill 250–350 m deep (Smith and Sandwell 1997; Murray and Arief 1988), observational evidence indicates that a reasonable choice of upper layer for a 1½-layer model of the region would lie almost entirely above the sill. In this case, theoretical results of Killworth (1989) indicate that a low-frequency, linear Kelvin wave in the interface would propagate over the sill with minimal loss of energy. All available long-term moored current measurements indicate that the flow variability along the southern coast of the Indonesian archipelago is confined to the near-surface layer. For example, measurements reported by Molcard et al. (1994) near Savu Strait, Molcard et al. (1996) in Timor Passage, Molcard et al. (2001) in Ombai Strait, and Sprintall et al. (2000) on the south coast of Java all show the variability to occur predominantly above about 300 m. An analysis of current meter measurements and repeat STD casts by Murray and Arief (1988) indicated that 80% of the transport in Lombok Strait occurs above

Corresponding author address: Ted Durland, Department of Oceanography, University of Hawaii at Manoa, 1000 Pope Road, Honolulu, HI 96822.
E-mail: tdurland@soest.hawaii.edu

the 200-m level and that none of the flow above the 300-m level is blocked by the sill. Sprintall et al. (2000) demonstrated that a simple analytical model for Kelvin wave generation and propagation forced by ECMWF winds along the equatorial and coastal waveguide from the western equatorial Indian Ocean to Lombok Strait provides a remarkably good hindcast of the pressure signal north of the sill on the west side of Lombok Strait (Bali) when only the first vertical mode is considered. Higher vertical modes ''denigrate'' the correlation between model and observations. Given the above evidence it appears that the regional dynamics can be reasonably approximated by a 1½-layer model in which the interface lies predominantly if not entirely above the sill at the mouth of Lombok Strait. Killworth's (1989) results then lead us to expect the 1½-layer model to accurately predict the transmission of small amplitude waves through the Lombok Strait.

To gain insight into what determines the transmission of Kelvin waves through a strait, solutions were sought for a subinertial Kelvin wave governed by linearized, inviscid, 1½-layer f-plane dynamics, passing through an ''Ideal Strait,'' with square-corner mouths and straight, parallel channel walls (Fig. 1c). An approximate solution was found in three progressive steps, and describing the final solution in terms of these steps provides a clear insight into the basic physics of the problem.

1) Numerical solutions were first found for an

   ''Entrance'': A Kelvin wave in a semi-infinite sea is incident upon a semi-infinite channel that interrupts the coastline (Fig. 1a).

   For all channel widths, and for wave frequencies less than one-half the inertial frequency, the results can be approximated to a high degree of accuracy by a physically intuitive model with a simple mathematical expression.
2) Consideration of the time reversal invariance of the governing equations shows that the solution for an Entrance determines completely the solution for an

   ''Exit'': A Kelvin wave within a semi-infinite channel is incident upon the channel mouth where it opens into a semi-infinite sea (Fig. 1b).

   The solution shows that the energy transmission coefficients are identical for an Entrance and an Exit with the same channel width, and consequently an Exit with a channel narrow enough to be of interest will necessarily reflect some of the Kelvin wave energy back along the channel.
3) By combining an Entrance and an Exit with a connecting channel much longer than the Rossby radius, it is easy to show that the solution for an Ideal Strait involves a simple one-dimensional wave interference problem analogous to interference problems in other fields. Furthermore, numerical verification of the solution shows that the long channel length restriction can be relaxed with very little loss in accuracy.

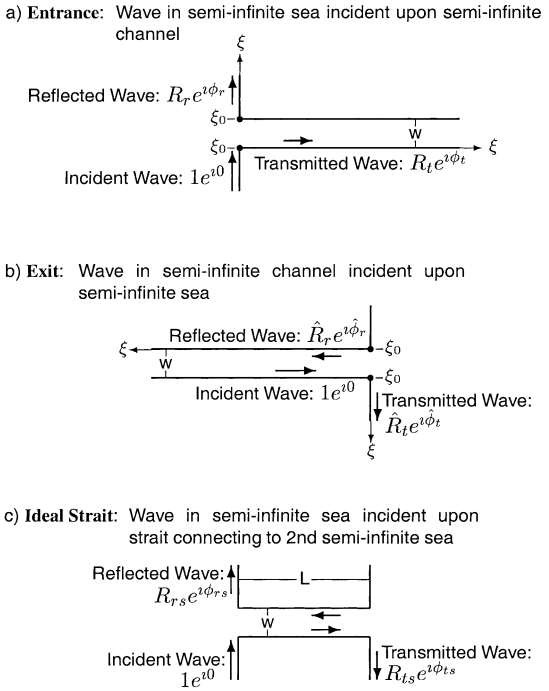

FIG. 1. Coastal configurations and radiation conditions for an Entrance, an Exit, and an Ideal Strait.

In what follows, the capitalized terms Entrance, Exit, and Ideal Strait will refer explicitly to the coastal configurations and radiation conditions shown in Figs. 1a–c. The goal of this study is the determination of the magnitude of the energy transmission coefficient for an Ideal Strait of any dimensions, and we focus on wave frequencies less than about 1/2 the inertial frequency for two reasons. Chong et al. (2000) and Potemra et al. (2002) analyzed three years of pressure gauge data from either side of Lombok Strait, and they found the most energetic spectral peaks within the 30–100-day period intraseasonal band, with numerous additional peaks in the 11–30-day band. The inertial period at Lombok Strait (8.5°S) is about 3.4 days, so frequencies less than 1/2 the inertial correspond to anything with a period greater than 7 days, and most of the intraseasonal band corresponds to frequencies less than 1/10 the inertial. Secondly, numerical solutions presented in section 3 will show that restricting the range of applicability to less than 1/2 the inertial frequency permits certain mathematical approximations that greatly simplify the formulation of the Ideal Strait solution while retaining a high degree of accuracy.

Problems involving Kelvin waves in channels date to G. I. Taylor's seminal work (Taylor 1920) dealing with the reflection of Kelvin waves from the end of a blocked channel. More recently, Packham (1969) used the Wie-

ner–Hopf technique to solve for superinertial Kelvin waves encountering an Exit, and Buchwald (1971) used a combination of Green's function, eigenfunction and conformal mapping techniques to solve the Entrance problem under the restriction that the channel width be small compared to both the wavelength and the Rossby radius. Buchwald and Miles (1974) presented an analytical solution for a Kelvin wave incident upon a gap in an infinitesimally thin barrier (strait of zero length) and Miles (1973) extended the solution technique to include an Ideal Strait of arbitrary length. Both of these solutions depend on the restriction that the strait width be small compared to the Rossby radius of deformation, and do so in ways that are not easy to extend to wider channels. This is not a problem when studying the barotropic waves of interest to Buchwald and Miles, but real deepwater strait widths are often of the same order as the first baroclinic mode Rossby radius, and the problem must be revisited in the study of baroclinic signals.

The solution obtained in this study has the advantages of clearly illuminating the physics involved in the problem, and of being highly accurate for all strait widths and lengths, and all substantially subinertial frequencies. The most obvious consequence of the solution is that transmission through an Ideal Strait is strongly dependent on kL (the product of wavenumber and channel length), so that two straits of identical width but different lengths transmit waves differently, and a given strait reacts differently to waves of different frequencies. The solution also demonstrates that an arbitrarily narrow strait can transmit virtually all of the energy at low frequency, as long as the linear and inviscid dynamics remain valid. This effect may be anticipated by considering the geostrophic limit, but what may be surprising is that an example with geometry and latitude similar to the Lombok Strait shows this limit being approached even in the middle of the intraseasonal band, confirming the results of Qiu et al. (1999).

After an introduction to the governing equations and terminology in section 2, the solutions are presented in section 3 and the consequences discussed in section 4. In section 5 numerical solutions are found on both the f plane and the β plane for a strait with coastal geometry similar to Lombok Strait. The numerical solutions are compared with the Ideal Strait solution and consequences of the solution relevant to Lombok are discussed. Section 6 compares model predictions with observations, and results are summarized in section 7.

2. Equations and terminology

The dynamical model considered here consists of the unforced, linear, inviscid, 1½-layer reduced-gravity equations on an f plane:

$$u_t - fv + g'\zeta_x = 0 \tag{1}$$

$$v_t + fu + g'\zeta_y = 0 \tag{2}$$

$$\zeta_t + h(u_x + v_y) = 0, \tag{3}$$

where u and v are the zonal and meridional velocities, f is the inertial frequency, h is the equilibrium upper-layer thickness, ζ is the interface displacement from equilibrium, and g' is the reduced gravity. Where required, numerical solutions to (1)–(3) are found using a centered space, leap frog time finite-difference scheme on a staggered C grid, with a Matsuno time step used periodically to control the computational mode. Spatial resolution is $\Delta x = \Delta y = 0.05\mathcal{R}$, where $\mathcal{R} \equiv c_p/f$ is the first mode baroclinic Rossby radius and c_p is the first-mode phase speed. The script $\mathcal{R}$ is used to distinguish the Rossby radius from the R used to denote amplitude ratios. Temporal resolution is $\Delta t = (\Delta x/\mathcal{R})/(4f)$.

The terms in Fig. 1 bear some explanation. The designation of the reflected wave at the Entrance (Fig. 1a) may not be intuitively obvious, but a fundamental correspondence exists between this wave and the reflected wave at the Exit. This will be brought out in the next section, and the given labeling of incident, transmitted and reflected waves provides the best consistency between the two solutions. The labeling for the Ideal Strait follows logically. Here, R and ϕ are the magnitude and phase of the complex amplitude of the solution:

$$\zeta = \Re[Re^{i\phi}e^{i(k\xi-\omega t)}e^{-\mathrm{sgn}(f)\eta/\mathcal{R}}], \tag{4}$$

where $\Re$ denotes the real part, k and ω are the wavenumber and wave frequency, ξ is a wave-following coordinate that increases in the direction of propagation and whose axis coincides with the shore to which the wave is trapped, and η is a cross-shore coordinate on an axis 90° counterclockwise from the ξ axis. The amplitude ($Re^{i\phi}$) is the Kelvin wave amplitude on the ξ axis. The last exponential in (4) represents the offshore amplitude decay along a strait coastline, where $\mathrm{sgn}(f) \equiv f/|f|$ gives the hemisphere-dependent sense of the decay. The incident wave is assigned unit amplitude and zero phase in all cases, so the R represent amplitude ratios and the ϕ represent phase shifts. With the above representation, a positive value for ϕ indicates a phase lag. The subscript r denotes the reflected wave while the subscript t denotes the transmitted wave. The factors for the Exit are distinguished from those of the Entrance by a hat, and the factors for the strait are distinguished by an additional subscript s. The symbol W is the channel width in all cases, and L is the length of the strait.

Because ξ is a wave-following coordinate, the transmitted wave and the reflected wave each gets its own ξ axis. A depiction of these axes and how they match up at a common origin, ξ_0, is given in Fig. 1a for the Entrance and Fig. 1b for the Exit.

A convenient feature of the given dynamics is that the only propagating wave solution in the subinertial range is the Kelvin wave. Consequently, energy flux in the Kelvin wave mode is conserved, and knowledge of only one of R_r or R_t fixes the other. Poincaré modes are excited near the channel mouths to help satisfy the boundary conditions there, but they are trapped to and decay away from the channel mouths. In this study we

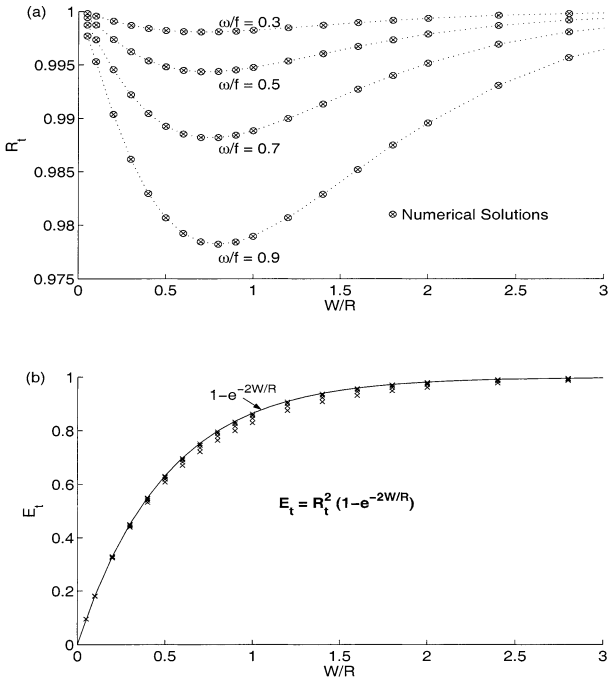

FIG. 2. Entrance: (a) transmitted wave amplitude ratio R_t and (b) energy transmission ratio E_t vs ratio of channel width to Rossby radius $W/\mathcal{R}$ at selected wave frequencies. The individual points in (b) correspond to the numerical solutions in (a).

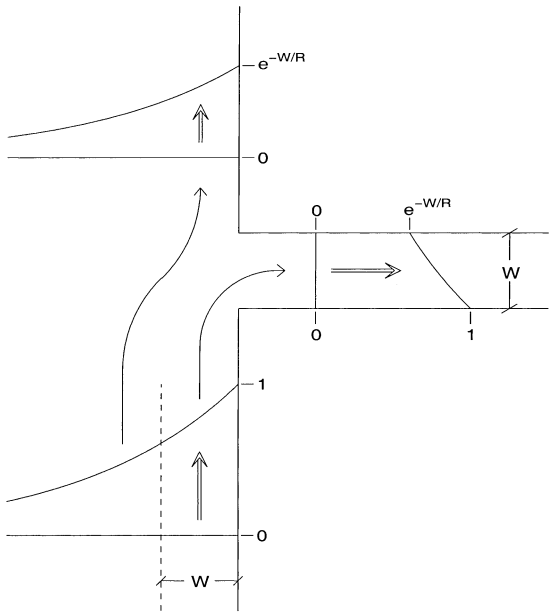

FIG. 3. Entrance: approximate solution. Vertical amplitude profiles are displayed in the horizontal plane. Kelvin wave rounds the corner into the channel with amplitude at wall unchanged. Offshore profile is truncated by opposite side of channel.

are concerned only with the propagating solution and we ignore what we call the ''adjustment solution''—the difference between the full solution and the pure Kelvin wave signal near the channel mouth. As a result, the amplitudes and phases are treated as though they change discontinuously at the channel mouths, and (4) represents the wave at some distance from the channel mouth. The decay scale for the adjustment solution is of the order of the Rossby radius along the open coast, but is much smaller within the channel where the flow is constrained by the channel walls. Consequently, the solutions obtained by neglecting the adjustment solution remain highly accurate within the channel even very close to the mouth. This is confirmed numerically in section 4d.

Results are presented in terms of the nondimensional parameters ω/f, $W/\mathcal{R}$, and kL.

3. Solutions

a. Entrance

The Entrance solution is achieved numerically by generating a pure sinusoidal Kelvin wave at a boundary 15 Rossby radii distant from the channel mouth. When the front of the resulting wave train encounters the channel mouth, some energy is lost to higher-frequency free Poincaré modes, and the transmitted and reflected Kelvin wave signals are allowed to stabilize before measuring the amplitude ratios and phase shifts. At frequencies less than $f/2$ this happens quite rapidly.

Figure 2a shows the numerical solutions for R_t over a range of $W/\mathcal{R}$ and ω/f values. Note that R_t may be approximated as 1 for all values of $W/\mathcal{R}$ with very little error, as long as the wave frequency does not approach the inertial frequency. Specifically, for frequencies less than $f/2$ the maximum error in this approximation is about 0.5%, corresponding to a 1% error in the energy flux approximation. To emphasize this, Fig. 2b shows the energy transmission coefficient versus channel width curve based on $R_t = 1$, and the actual transmission coefficients based on the numerical solutions shown in Fig. 2a. The points falling farthest from the continuous curve represent the solutions for $\omega/f = 0.9$. Most baroclinic Kelvin waves of interest are substantially subinertial, and the frequencies of interest at Lombok Strait fall well below $f/2$ (see the introduction).

As a physically intuitive mnemonic for the approximate solution, the Kelvin wave at an Entrance may be thought of as rounding the corner into the channel with no change in amplitude, and simply having its offshore amplitude profile truncated by the opposite shoreline (Fig. 3). The approximate Entrance amplitude ratios are

$$R_t = 1, \tag{5}$$

$$R_r = e^{-W/\mathcal{R}}. \tag{6}$$

In what follows this approximation will be used with the understanding that the amplitude factors shown in Fig. 2a could always be applied for a higher degree of accuracy.

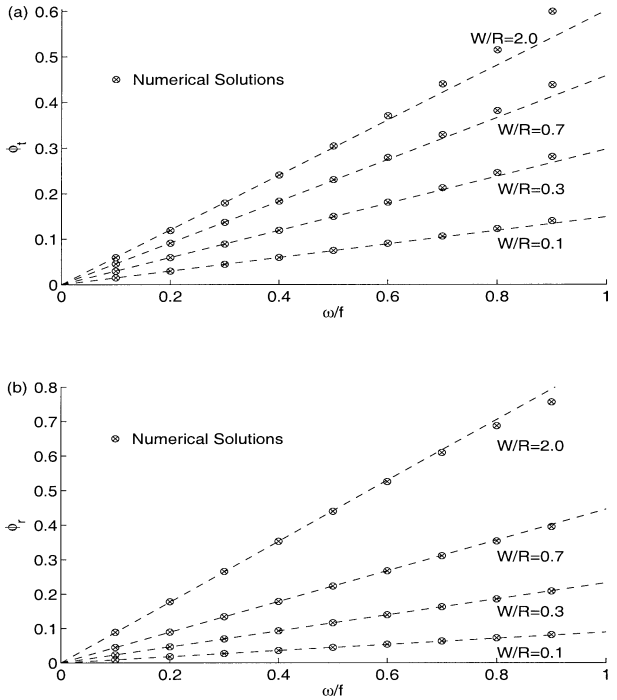

FIG. 4. Entrance: transmitted and reflected wave phase shifts (a) ϕ_t and (b) ϕ_r vs ratio of wave to inertial frequency ω/f at selected values of channel width to Rossby radius ratio $W/\mathcal{R}$. Dashed curves are straight lines through the origin and numerical solutions at $\omega/f = 0.4$.

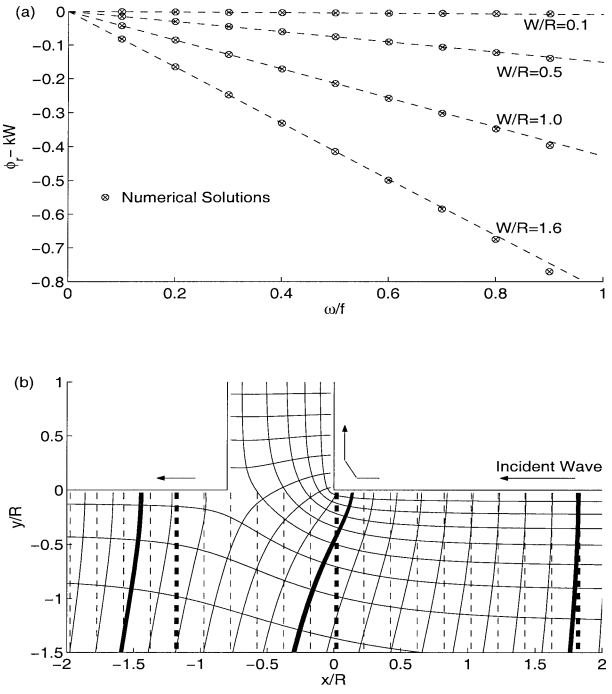

FIG. 5. (a) Reflected wave phase shift measured along continuous axis across Entrance channel $\phi_r - kW$ vs ratio of wave to inertial frequency ω/f. Negative values indicate phase advance. (b) Solid lines represent corange and cophase contours for Entrance scenario with $W/\mathcal{R} = 0.8$ and $\omega/f = 0.3$. Dashed lines represent cophase contours for wave propagating along an unbroken coast. The three pairs of heavy lines represent cophase contours with the phase value equal for solid and dashed contours. Pivoting of the wave around the near corner of the channel mouth results in the phase reaching the distant shore earlier than it would in the case of the unbroken coast.

The numerical solutions for the phase shifts ϕ_t and ϕ_r are plotted versus ω/f in Figs. 4a and 4b, respectively, for selected values of $W/\mathcal{R}$. Both ϕ_t and ϕ_r are nearly linear in ω/f, implying that an Entrance is very nearly nondispersive. The nondispersive assumption is particularly good for frequencies less than $f/2$ and we will use this approximation in what follows, allowing the phase shifts to be expressed as the product of ω/f and the $W/\mathcal{R}$-dependent solutions at a given frequency. We use $\omega/f = 0.4$ as this ''standard'' frequency and the dashed curves in Figs. 4a and 4b are straight lines through the origin and the numerical solutions at $\omega/f = 0.4$. This choice provides the least sum of absolute errors over the range $0.1 \leq \omega/f \leq 0.5$ and very nearly the least error over the range $0.1 \leq \omega/f \leq 0.6$ for both ϕ_t and ϕ_r. The $W/\mathcal{R}$ dependence of the phase shifts will be presented in section 3c after the Exit phase shifts have been addressed.

Note that ϕ_r is defined relative to the special wave-following coordinate system shown in Fig. 1, which was defined for convenience of the analysis to follow in section 3b. The phase shift relative to a continuous axis across the channel mouth is $\phi_r - kW$ (where k is the wavenumber and W the channel width) and this is plotted in Fig. 5a. As an aside, it is interesting to note that this phase shift is negative for all values of ω/f and $W/\mathcal{R}$, implying a phase advance: the phase reaches the coast past the channel sooner than it would in the absence of a channel. This is illustrated in Fig. 5b for the values $\omega/f = 0.3$ and $W/\mathcal{R} = 0.8$. The corange and cophase contours for the Entrance scenario are represented by solid lines, while the cophase contours for a no-channel scenario are represented by dashed lines. Three different values of the phase are accented with extra thick lines to emphasize the difference between the two scenarios. As the wave approaches the channel, the phase at the coast is retarded but, because the wave pivots around the near corner of the channel mouth, the phase propagation in the vicinity of the mouth resembles that of the classical solution for a wave trapped to a cylindrical coast (Longuet-Higgins 1969). It is the angular phase speed that is approximately constant in this region so that the linear phase speed of the offshore source of the reflected wave exceeds the phase speed of a wave propagating along an unbroken coastline.

b. Exit

The analysis of the Exit proceeds by noting that the governing equations are invariant under a time reversal, $(\partial_t, u, v, f) \rightarrow (\partial_{-t}, -u, -v, -f)$ [or more appropriately $(\partial_{-t}, u, v, f) \rightarrow (\partial_t, -u, -v, -f)$] so that a movie of

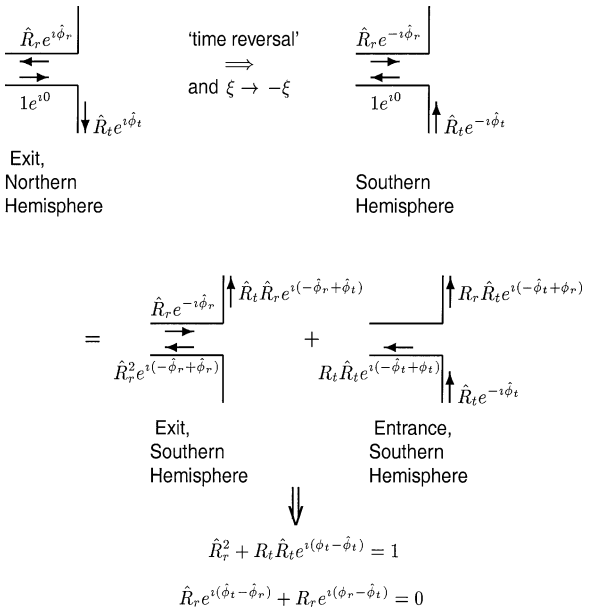

FIG. 6. Time reversal connection between an Exit and an Entrance. Using the time reversal invariance of the governing equations, an Exit can be transformed into a linear combination of an Entrance and an Exit, allowing the complex transmission and reflection coefficients for an Exit to be derived from those of an Entrance.

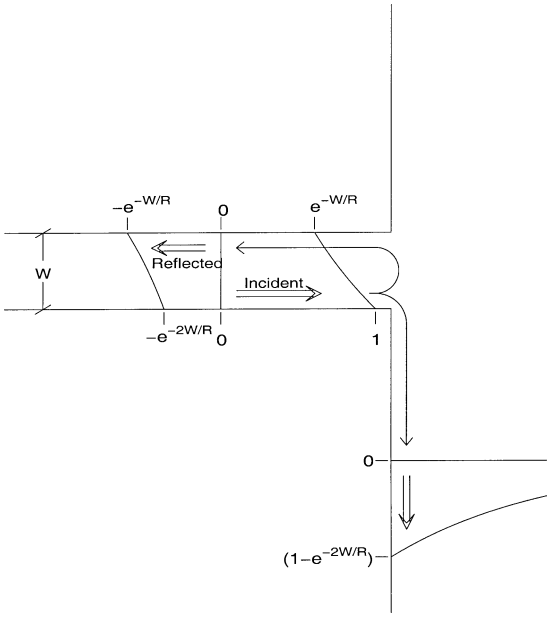

FIG. 7. Exit: approximate solution. Vertical amplitude profiles are displayed in the horizontal plane. Open sea provides a fixed boundary condition at the far corner of the Exit mouth (the corner around which the Kelvin wave *cannot* propagate). Incident and reflected waves cancel each other at this corner.

a Kelvin wave played backward would appear to be a dynamically correct movie of a Kelvin wave in the opposite hemisphere traveling in the opposite direction. This applies not only to the pure Kelvin wave signal, but to all dynamical modes, specifically the adjustment solution trapped to the channel mouth. Consequently, the picture for the Exit (Fig. 1b) can be ''time reversed'' by changing the directions of the arrows and changing the signs of $\hat{\phi}_r$ and $\hat{\phi}_t$ (because the direction of ξ is reversed). This situation is shown in Fig. 6. Because the problem is linear, the time-reversed situation can be viewed as a superposition of two incident waves in the Southern Hemisphere, one representing an Entrance scenario and the other an Exit scenario, with the solution to the combination specified. With the Entrance and presumed Exit complex reflection and transmission amplitude ratios applied to the two incident waves, the following relationships can be derived specifying the Exit solution completely in terms of the Entrance solution:

$$\hat{R}_r = R_r \tag{7}$$

$$\hat{R}_t = R_t(1 - e^{-2W/\mathcal{R}}) \tag{8}$$

$$\hat{\phi}_r = 2\phi_t - \phi_r + \pi \tag{9}$$

$$\hat{\phi}_t = \phi_t. \tag{10}$$

Conservation of energy flux gives

$$(1 - R_r^2) = R_t^2(1 - e^{-2W/\mathcal{R}}) \tag{11}$$

$$(1 - \hat{R}_r^2) = \hat{R}_t^2/(1 - e^{-2W/\mathcal{R}}). \tag{12}$$

In addition, energy transmission coefficients may be defined as the ratio of transmitted to incident energy flux, and

$$E_t = R_t^2(1 - e^{-2W/\mathcal{R}}) \tag{13}$$

$$\hat{E}_t = \hat{R}_t^2/(1 - e^{-2W/\mathcal{R}}) = E_t. \tag{14}$$

This last result deserves further comment. The fraction of the incident energy that propagates out of an Exit of a given width is identical to the fraction of the incident energy that propagates into an Entrance of the same width. Because (7)–(14) are exact, Fig. 2b also represents the energy transmission coefficient plot for an Exit, both for the $R_t = 1$ approximation and for the frequency-dependent numerical solutions.

A physically intuitive mnemonic for the approximate solution at an Exit is to think of the open sea as providing a fixed boundary condition at the corner of the channel mouth around which the incident wave *cannot* propagate. This induces a reflection back along the channel with a 180° phase shift, and with the major amplitude of the reflected wave equal to the minor amplitude of the incident wave (Fig. 7). This view is a conceptual extension of Lighthill's (1978) treatment of one-dimensional waves at a channel discontinuity in a nonrotating system.

The approximate Exit amplitude ratios are

$$\hat{R}_t = 1 - e^{-2W/\mathcal{R}}, \tag{15}$$

$$\hat{R}_r = e^{-W/\mathcal{R}}. \tag{16}$$

c. Ideal Strait

An Ideal Strait may now be constructed by considering an Entrance at the incident end of the strait and an Exit at the other end. For simplicity, we will call these ends respectively the ''inlet'' and ''outlet.'' Of course the inlet is an Entrance only to the incident wave. Part of the wave transmitted into the channel at the inlet will be reflected from the outlet, return to see the inlet as an Exit, and set up an endless ''internal reflection'' process. The channel wave will combine with the incident wave after one round trip, resulting in a wave interference problem. If the length of the strait is greater than or equal to $\mathcal{R}$, the adjustment solution trapped to the inlet is negligible at the outlet, and the reflection coefficients obtained for the semi-infinite channels of an Entrance and an Exit will be valid for the inlet and outlet of the strait. This is presumed to hold in what follows.

Wave interference problems are most easily posed in terms of harmonic time-dependence, but because baroclinic signals are frequently eventlike, it is instructive to see how the solution sets up by viewing the Ideal Strait as being impinged upon by a semi-infinite sinusoidal wave train with a distinct wave front similar to the one generated numerically for the Entrance solution. As mentioned in section 3a, the energy lost to higher-frequency modes at the front of the wave train is negligible for primary frequencies less than $f/2$, and we will neglect this effect. As the wave front enters the inlet, the amplitude is attenuated by R_t. If we now follow only the part of the wave that remains in the channel through the internal reflections, the effect of one round trip of the channel can be expressed as a complex amplitude attenuation factor:

$$C = \hat{R}_r^2 e^{i\alpha}, \tag{17}$$

where

$$\alpha = 2(\hat{\phi}_r + kL) \tag{18}$$

is the phase shift that the channel wave experiences in one round trip. At this point the attenuated channel wave combines linearly with the still incoming incident wave, and the process is repeated, producing a geometric series in C. The number of terms in the series corresponds to the number of round trips completed by the wave train. If time t is measured from when the wave front enters the inlet, then the wave emerging from the outlet will have experienced N ($N = 0, 1, 2, \ldots$) recombinations with the incident wave when

$$[L + 2N(L + W_e)]/c_p < t < [L + 2(N + 1)(L + W_e)]/c_p, \tag{19}$$

and it will have an amplitude ratio of

$$R_{ts}(N) = R_t \hat{R}_t \left| \sum_{n=0}^{N} C^n \right|. \tag{20}$$

In (19) the term W_e is an equivalent width that accounts for the time absorbed by the Exit reflection.

For the remainder of this section we will only be concerned with the fully converged solution ($\lim_{N\to\infty}$), and that is straightforward to calculate:

$$R_{ts} = R_t \left| \frac{1}{1 - C} \right| \hat{R}_t = \frac{R_t \hat{R}_t}{(1 - 2\hat{R}_r^2 \cos\alpha + \hat{R}_r^4)^{1/2}}. \tag{21}$$

Using the relations between the Entrance and Exit parameters, (7)–(14), (21) can be written more compactly as

$$R_{ts} = \left\{ 1 + \left[\frac{2R_r \sin(\alpha/2)}{(1 - R_r^2)} \right]^2 \right\}^{-1/2}, \tag{22}$$

and the energy transmission ratio for the strait is then

$$E_{ts} = R_{ts}^2 = \left\{ 1 + \left[\frac{2R_r}{(1 - R_r^2)} \sin\left(\frac{\alpha}{2}\right) \right]^2 \right\}^{-1}. \tag{23}$$

The problem is equivalent to the classical optics problem of multiple beam interference due to partial reflection from two parallel plates, and (23) is identical in form to the optics solution presented by Longhurst (1967).

In this paper we are primarily concerned with the energy transmission ratio, but for completeness the reflected wave amplitude ratio and the phase shifts are

$$R_{rs} = R_r \left| \frac{1 - e^{i\alpha}}{1 - C} \right| = \left\{ 1 + \left[\frac{(1 - R_r^2)}{2R_r \sin(\alpha/2)} \right]^2 \right\}^{-1/2} \tag{24}$$

$$\begin{aligned} \phi_{ts} &= 2\phi_t - \arg(1 - C) \\ &= 2\phi_t + \tan^{-1}\left(\frac{R_r^2 \sin\alpha}{1 - R_r^2 \cos\alpha} \right) \end{aligned} \tag{25}$$

$$\begin{aligned} \phi_{rs} &= \phi_r + \arg\left(\frac{1 - e^{i\alpha}}{1 - C} \right) \\ &= \phi_r - \tan^{-1}\left[\frac{(1 - R_r^2) \sin\alpha}{(1 + R_r^2)(1 - \cos\alpha)} \right]. \end{aligned} \tag{26}$$

Using the low-frequency approximation (6) for R_r, (23) can be written

$$E_{ts} = \left\{ 1 + \left[\frac{\sin(\alpha/2)}{\sinh(W/\mathcal{R})} \right]^2 \right\}^{-1}. \tag{27}$$

Because $\alpha/2$ appears in a $\sin^2$ term, (27) remains unchanged if $\alpha/2 = (\hat{\phi}_r + kL)$ is replaced by $(\hat{\phi}_r - \pi + kL)$. Subtracting π from $\hat{\phi}_r$ merely deletes the 180° phase shift associated with the Exit reflection, so

$$\hat{\phi}_r - \pi = kW_e = (\omega/f)(W_e/\mathcal{R}), \tag{28}$$

where W_e is the equivalent width in (19) that represents the time delay in the Exit reflection. Because ϕ_t and ϕ_r can be expressed as the product of ω/f and width-de-

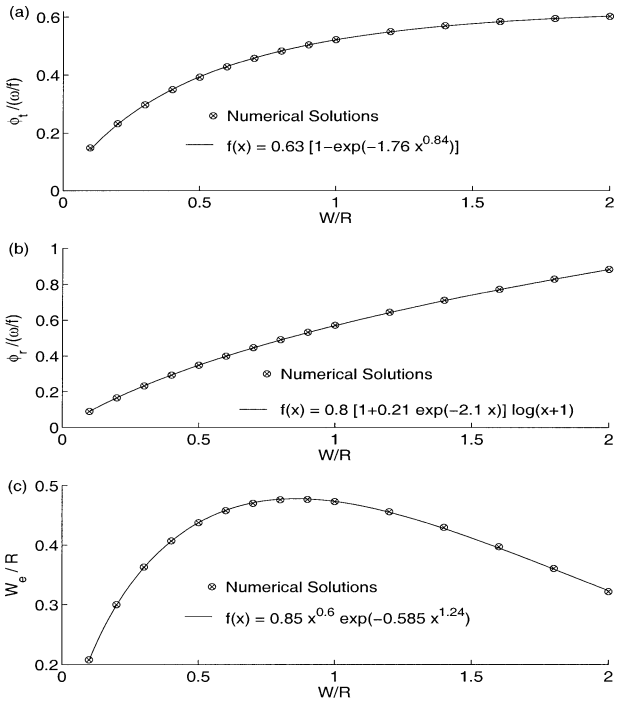

FIG. 8. Dependence of phase shifts on normalized channel width, W/R, based on numerical solutions at $\omega/f = 0.4$: (a) Entrance transmitted wave phase shift $\phi_t/(\omega/f)$, (b) Entrance reflected wave phase shift $\phi_r/(\omega/f)$, and (c) Exit reflected wave phase shift $[(\hat{\phi}_r - \pi)/(\omega/f)] = W_e/\mathcal{R}$ (normalized equivalent width). In each case the dependence on $W/\mathcal{R}$ is expressed as a function of x for notational simplicity. Given functions are meant only as a convenient interpolation within the range of numerical solutions and are not intended to have physical significance or extrapolative value.

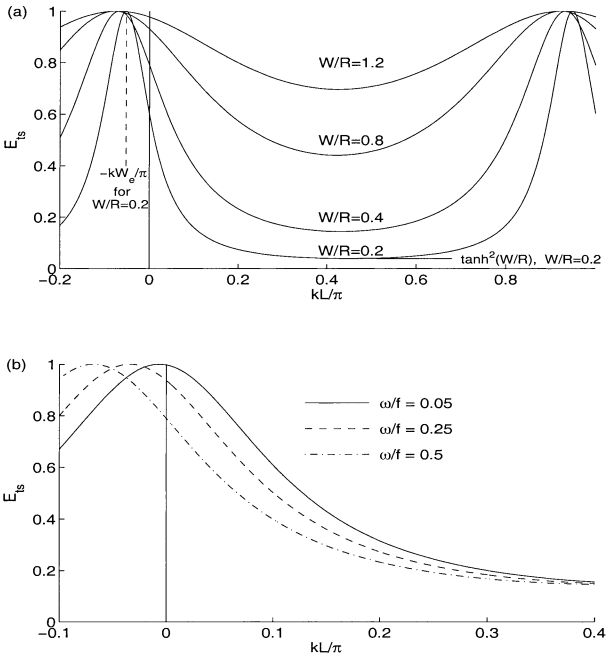

FIG. 9. Ideal Strait: (a) Energy transmission E_{ts} vs kL/π for $\omega/f = 0.5$ and various values of W/R. Note resonant character of solution and sensitive dependence on L near $kL = 0$. Also note that resonance peak near $kL = 0$ is at $kL = -kW_e$. (b) The E_{ts} vs kL/π for $W/R = 0.4$ and various values of ω/f. Note that resonance peak shifts toward $kL = 0$ as $\omega/f \to 0$.

pendent functions, this is also true of $\hat{\phi}_r - \pi = 2\phi_t - \phi_r$ [see (9)]. We can then write (27) as

$$E_{ts} = \left\langle 1 + \left\{ \frac{\sin[(\omega/f)(W_e/\mathcal{R} + L/\mathcal{R})]}{\sinh(W/\mathcal{R})} \right\}^2 \right\rangle^{-1}, \quad (29)$$

where W_e/R is a function only of W/R.

Figures 8a–c show the $W/\mathcal{R}$ dependence of $\phi_t/(\omega/f)$, $\phi_r/(\omega/f)$, and $(\hat{\phi}_r - \pi)/(\omega/f) = W_e/\mathcal{R}$. The numerical solutions are taken at $\omega/f = 0.4$ for the reasons given at the end of section 3a. Each plot is provided with a function that is meant only as a convenient interpolation within the range $0.1 \le W/\mathcal{R} \le 2.0$, and is not meant to have any physical significance or extrapolative value. The $W/\mathcal{R}$ dependence of $W_e/\mathcal{R}$ is approximated as

$$W_e/\mathcal{R} = 0.85(W/\mathcal{R})^{0.6} \exp[-0.585(W/\mathcal{R})^{1.5}]. \quad (30)$$

Together, (29) and (30) provide the solution for the energy transmission of a monochromatic Kelvin wave through an Ideal Strait after sufficient time has passed for full convergence. The time required for reasonable convergence is addressed in section 4f.

4. Consequences of strait solution and numerical verification

a. Functional form of E_{ts} versus kL

Figure 9a shows plots of E_{ts} versus kL for the single value of $\omega/f = 0.5$ and several values of $W/\mathcal{R}$. The curves extend to unphysical negative values of kL in order to demonstrate the resonant nature of the energy transmission solution. Examination of this figure and of (23) reveals the following general features:

$E_{ts}(kL + \pi) = E_{ts}(kL)$, transmission is periodic in kL

$$\max(E_{ts}) = \left(\frac{R_t \hat{R}_t}{1 - \hat{R}_r^2} \right)^2 = 1$$

$$\min(E_{ts}) = \left(\frac{R_t \hat{R}_t}{1 + \hat{R}_r^2} \right)^2 \approx \tanh^2\left(\frac{W}{\mathcal{R}} \right),$$

where $\approx$ indicates the use of the low-frequency approximations for R_t, $\hat{R}_t$, and $\hat{R}_r$: (5), (15), and (16).

The steepness of the curve near $kL = 0$ increases as $W/\mathcal{R}$ decreases.

The peak near $kL = 0$ is at $kL = -kW_e$. The choice of $\omega/f = 0.5$ in Fig. 9a maximizes the value of kW_e, thus emphasizing the offset of this peak from $kL = 0$. As discussed below, the peak shifts toward $kL = 0$ as $\omega/f \to 0$.

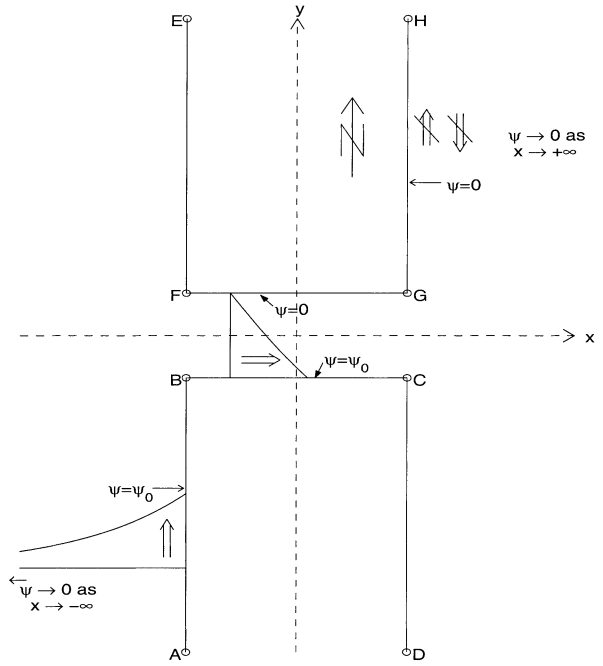

FIG. 10. Geostrophic steady state spun up from a single coastally trapped source of energy flux in the southwest quadrant. Impossibility of establishing a meridional energy flux in the northeast quadrant fixes the streamfunction on the opposite side of the strait at $\psi = 0$. Entire incident signal propagates through the strait.

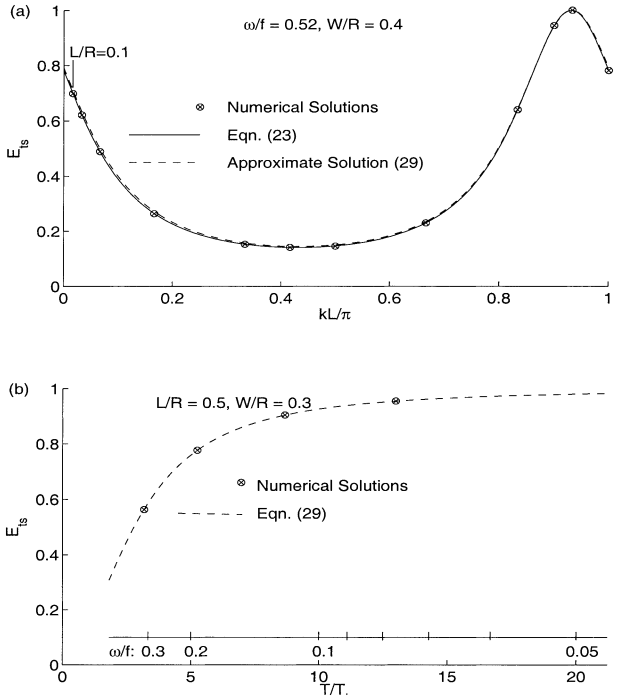

FIG. 11. Numerical verification of the energy transmission equation for an ideal strait: (a) The E_{ts} vs kL/π for $\omega/f = 0.52$ and $W/\mathcal{R} = 0.4$. Equation (29) uses the low-frequency approximations. (b) The E_{ts} vs the ratio of wave to inertial period T/T_i.

Aside from the values of the reflection factors, $\hat{R}_r$ and $\hat{\phi}_r$, the analysis of the previous section applies to the general problem of one-dimensional waves encountering two features in series that allow partial transmission and partial reflection. Resonant solutions similar to that shown in Fig. 7a are found in analyses of the optics problem of multiple beam interference (Longhurst 1967) and of quantum mechanical scattering from a finite square potential well (Griffiths 1995).

b. Sensitivity to channel length

Typical subinertial Kelvin waves have wavelengths much longer than realistic strait lengths, so the part of the resonance curve of most interest is that near $kL = 0$. For the wave frequency shown ($f/2$) this is where the curve is the steepest, and the energy transmission is therefore quite sensitive to differences in channel length.

c. Very low frequency limit

Because E_{ts} depends on the product of k and L, it appears that letting $k \to 0$ ($\omega \to 0$) is equivalent to letting $L \to 0$, but there is an important difference. For a given ω/f and $W/\mathcal{R}$, the position of the resonance peak is fixed, and the maximum value that E_{ts} can attain as $L \to 0$ may be significantly less than 1. As $\omega/f \to 0$ however, $kW_e \to 0$ and the resonance peak shifts toward 0 from below as $kL \to 0$ from above (illustrated in Fig. 9b). Thus $E_{ts} \to 1$ regardless of channel width and length.

This result may be anticipated by considering the geostrophic limit, $\omega = 0$, in which case the value of the streamfunction along a coastline is constant. Consider the situation in Fig. 10, where a geostrophic steady state has spun up from a single coastally trapped source in the southwest quadrant. Clearly the streamfunction $\psi \to 0$ as $x \to \pm\infty$ and $\psi = \psi_0$ along the entire coastline ABCD, where ψ_0 gives the northward alongshore energy flux at the source near A. In the northeast quadrant there is no southward energy flux by definition, and no propagating wave solutions exist that can set up a northward energy flux between the coast and $+\infty$. In the steady state, therefore, the streamfunction along the entire coastline EFGH has the value $\psi = 0$, and all of the energy propagates through the strait.

The above arguments assume, of course, that nonlinearities and/or dissipation remain negligible within the strait, which becomes less likely for smaller channel widths.

d. Numerical verification

To verify the energy transmission equations (23) and (29), Fig. 11a shows a plot of E_{ts} versus kL for the fixed

values $\omega/f = 0.52$ and $W/\mathcal{R} = 0.4$. The solid line is (23) with values for R_r and $\hat{\phi}_r$ interpolated from Fig. 2a [using (11)] and Fig. 8c, and the $\otimes$ are numerical solutions. The approximate solution, (29), has been plotted with a dashed line, and it is in good agreement with (23) as expected. Equations (23) and (29) compare well with the numerical solutions even for small values of $L/\mathcal{R}$. Comparisons with the existing analytical solutions for small channel widths show that for $\omega/f \leq 0.5$, the maximum discrepancy as $L \to 0$ is about 2%. The choice of $\omega/f = 0.52$ is above the top end of our validity range, $\omega/f \leq 0.5$ and thus provides a worst case. Agreement between the model and numerical solutions will be even better at lower frequencies.

To verify the frequency dependence and emphasize the low-frequency approach to total transmission, Fig. 11b shows E_{ts} versus T/T_i for the fixed values $W/\mathcal{R} = 0.3$ and $L/\mathcal{R} = 0.6$, where T is the wave period and T_i the inertial period. The dashed line represents (29) and the $\otimes$ are numerical solutions. Again the agreement is good. We see that the energy transmission of this particular Ideal Strait configuration is quite sensitive to wave frequency between $T/T_i = 2$ ($E_{ts} \approx 0.3$) and $T/T_i = 6$ ($E_{ts} \approx 0.8$). Above $T/T_i = 2$, E_{ts} increases monotonically as $T \to \infty$, with $E_{ts} > 0.9$ for $T/T_i > 10$.

e. Cross-channel decay

The existence of the Exit internal reflection means that the Ideal Strait contains two Kelvin waves traveling in opposite directions. For $kL \ll 1$ each wave has essentially a constant phase along the length of the Ideal Strait, but the two waves are roughly 180° out of phase with each other. The pressure decay across the Ideal Strait (and hence the strength of the currents within the Ideal Strait) is consequently greater than would be expected from a single Kelvin wave propagating along the channel, consistent with $E_{ts} \to 1$. This also means that the pressure at the downstream channel wall (farthest from the energy source) is less sensitive than might be expected to the incident signal.

f. Convergence

Equations (23), (27), and (29) are for the fully converged solution, and we are frequently interested in pulse-like incident signals, so it is important to assess how rapidly the solution converges. Because the solution is determined by a geometric series in the complex attenuation coefficient $\mathcal{C}$ (see section 3c), this is straightforward to estimate. After N round trips within the Strait, the relative difference between the truncated and the fully converged solution is

$$\left|\frac{E_{ts\infty} - E_{tsN}}{E_{ts\infty}}\right| = \left|\frac{\left|\sum_{n=0}^{\infty} \mathcal{C}^n\right| - \left|\sum_{n=0}^{N} \mathcal{C}^n\right|}{\left|\sum_{n=0}^{\infty} \mathcal{C}^n\right|}\right| \leq \left|\frac{\sum_{n=0}^{\infty} \mathcal{C}^n - \sum_{n=0}^{N} \mathcal{C}^n}{\sum_{n=0}^{\infty} \mathcal{C}^n}\right| = |\mathcal{C}^{N+1}| = \hat{R}_r^{2(N+1)} \approx e^{-2(N+1)W/\mathcal{R}}, \quad (31)$$

with the approximation symbol implying the use of (16) for $\hat{R}_r$. In section 5, an Ideal Strait with transmission characteristics similar to a strait with Lombok's coastal geometry is found to have $L/\mathcal{R} = 0.83$ and $W/\mathcal{R} = 0.23$ ($W_e/\mathcal{R} = 0.33$). Seven round trips would bring the solution to within 2% of convergence and with $\mathcal{R} = 111$ km and $c_p = 2.4$ m s^{-1}, this would take less than 9 days. This is fairly short in comparison with intraseasonal periods or with the duration of the 1-month-long pulse observed by Sprintall et al. (2000), and so the fully converged solution presented here should be applicable to events of these timescales.

5. Application to an idealized Lombok Strait

To evaluate the utility of the Ideal Strait model in approximating more geometrically complex straits, numerical solutions are calculated for a strait with coastal geometry based on the Smith and Sandwell (1997) 200-m isobath at the Lombok Strait. The calculations are based on a 1½-layer model and do not include the effect of the sill.

Figure 12a shows the results (○) of numerical calculations of the energy transmission coefficient for the modeled strait at four different wave periods: 11, 22, 33, and 55 days. Figures 12b and 12c show the coastline and the corange contours for the 11- and 55-day-period results. The first-mode Rossby radius is taken to be 1° latitude at 8.5°S, corresponding to a phase speed of 2.4 m s^{-1}, which compares well with the observed phase speed of 2.5 m s^{-1} reported by Chong et al. (2000). The convergence of meridians is ignored (<2% distortion in Δx at 9°S), and the model resolution is 1/30° latitude by 1/30° longitude. Note that $E_{ts} = 0.92$ at $T = 55$ days, and increases monotonically as the period increases.

Figure 12a also shows the plots of the energy transmission equation (29) for several Ideal Straits with the same length as the modeled strait ($L = 0.83\mathcal{R} = 0.83°$ lat). The plot for $W = 0.23\mathcal{R}$ matches the numerical solutions well, showing that the more complex strait does indeed have transmission characteristics equivalent to an Ideal Strait of a given width (W_I). Determining the appropriate width, however, is not a trivial matter. The plots for two simple-minded attempts at estimating

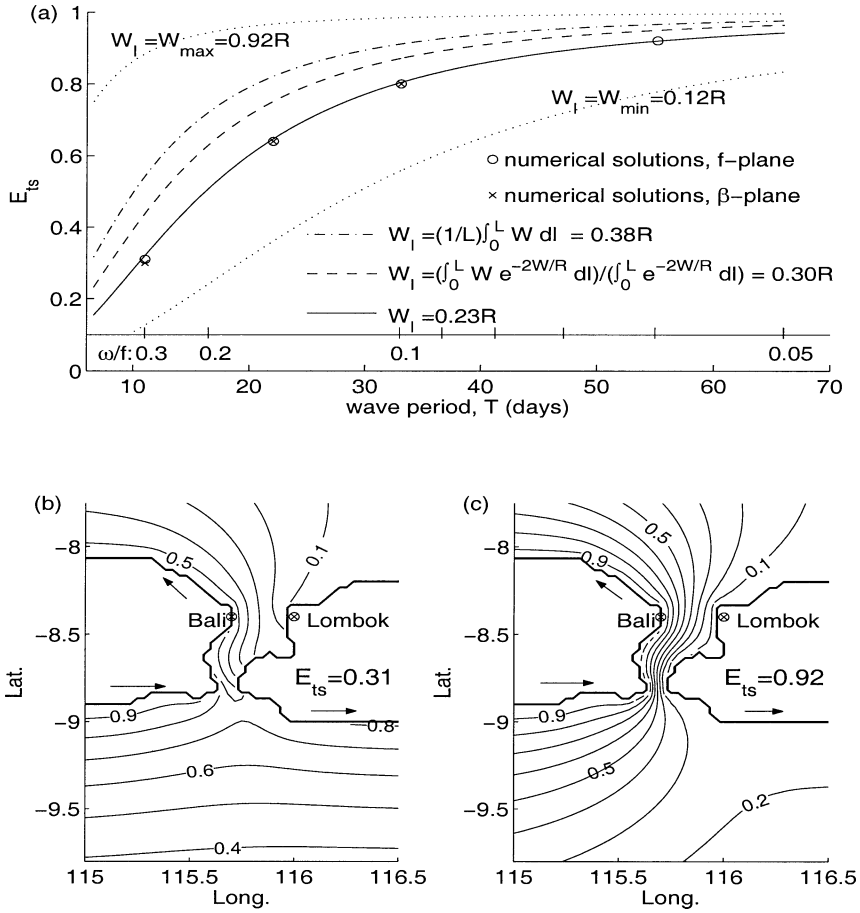

FIG. 12. Energy transmission for a strait based on Lombok Strait 200-m contour. (a) The E_{ts} vs wave period T for actual strait (numerical solutions) and various ideal straits of different widths [Eq. (29) with $L = 0.83\mathcal{R}$]. (b) Corange contours for $T = 11$ days. Bali and Lombok pressure gauge locations (Potemra et al. 2002) identified by circled ×. (c) Same as (b) but for $T = 55$ days.

this effective width are shown: an average over the length of the strait giving $W_I = 0.38\mathcal{R}$, and a weighted average using the Kelvin wave energy flux decay as a weighting function (to emphasize the narrower parts of the strait), giving $W_I = 0.30\mathcal{R}$. These estimates leave something to be desired, but they are at least in the ballpark. Perhaps the most interesting feature of the plot is the amount of information contained in the two outermost dotted curves. The upper curve represents an Ideal Strait with an effective width, $W_I = 0.92\mathcal{R}$, equal to the maximum width over the length of the modeled strait, while the lower curve represents an Ideal Strait with the minimum width, $W_I = 0.12\mathcal{R}$. Even with such a wide window of uncertainty it is clear that the modeled strait will approach the total transmission condition within the intraseasonal period band (30–100 days).

A reasonable question to ask is how well one would expect an f-plane model to predict the behavior of a strait within 10° of the equator? To partially address this concern, numerical solutions are calculated for the above modeled strait on a β plane at the three wave periods: 11, 22, and 33 days. The results (×) are shown in Fig. 12a, and they can be seen to be virtually identical to the f-plane results. Although it is now possible for energy to leak from the Kelvin wave into Rossby wave modes, the f-plane dynamics still seem to provide a good prediction of the transmission characteristics of the strait. The full β-plane solution of course requires a complete understanding of the energy transfer between Kelvin and Rossby modes along irregular, nonmeridional boundaries and we can only speculate that the predictive success of the f-plane model is due to the Kelvin wave adjustments inherent in the solution occurring much faster than any possible mode conversions within the strait.

6. Validity of model and comparison with observations

We have found solutions for a 1½-layer, linear, inviscid model that have illuminated the most basic dynamics of Kelvin wave transmission through a strait,

and we have presented the model's predictions for Lombok Strait. Unfortunately, some of the basic assumptions of the model are often violated at Lombok Strait, and we now look at which aspects of the model predictions might remain useful, and how other aspects might be modified in the face of more complicated dynamics.

a. Cross-strait decay scale

Perhaps the most robust prediction of the solution, and one that might not otherwise have been expected, is the increase in the cross-channel pressure decay as a consequence of the Exit reflection and its 180° phase shift. Analogs to the Exit behavior are found in all branches of physics where a propagating wave encounters an abrupt change in the domain, and the enhanced cross-channel decay prediction seems to be supported by the pressure gauge data presented by Potemra et al. (2002). The locations of their Bali and Lombok pressure gauge stations, spanning the outlet of Lombok Strait (for a wave of Indian Ocean origin), are shown in Figs. 12b and 12c. Although it is often difficult to distinguish between the effects of local forcing, remote Indian Ocean forcing and remote Pacific Ocean forcing, Fig. 7 in Potemra et al. (2002) identifies five spikes in the pressure signals at these stations that are not well correlated with local winds but are well correlated with westerly wind forcing in the central equatorial Indian Ocean at a lag time appropriate for Kelvin wave propagation. Their Fig. 4 shows concurrent time series of the pressure signals at Bali and Lombok and the cross-strait pressure difference between the two stations, Δp, which was calibrated with ADCP sections (Hautala et al. 2001). Given that the distance between the two stations is about $0.28\mathcal{R}$, an $e^{-W/\mathcal{R}}$ decay across the strait would lead one to expect a ratio between the amplitudes of the Δp signal and the Bali pressure signal of about 0.25. Figure 4 in Potemra et al. (2002), however, shows that this ratio ranges from 0.75 to 1 for the five events identified as remotely forced Kelvin waves, supporting the prediction of an enhanced cross-channel decay. In Fig. 13 we have reproduced the time series for the Bali (upper, solid line) and Lombok (lower, dashed line) pressure signals during three of these events. The signals have each been shifted to zero at the onset of the event in an attempt to view only the amplitude of the remotely forced pulse. A dotted line has been added to each plot at 75% of the Bali signal, showing the response that would be expected at the Lombok gauge if the cross-strait decay were exponential with a Rossby radius decay scale. In each case the observed cross-channel decay is significantly greater.

Potemra et al. (2002) make the point that the cross-strait pressure difference variations are poorly correlated with the Lombok pressure variations, and this is in accord with the predictions of our solution. For waves originating in the Indian Ocean, the Lombok station is located near the far side of the outlet and we expect the incident wave and Exit reflection to nearly cancel each other at this location, making the Lombok gauge relatively insensitive to Indian Ocean signals. In our Fig. 12b this is seen to be true even at the short period of 11 days, for which the transmission coefficient is only 0.31.

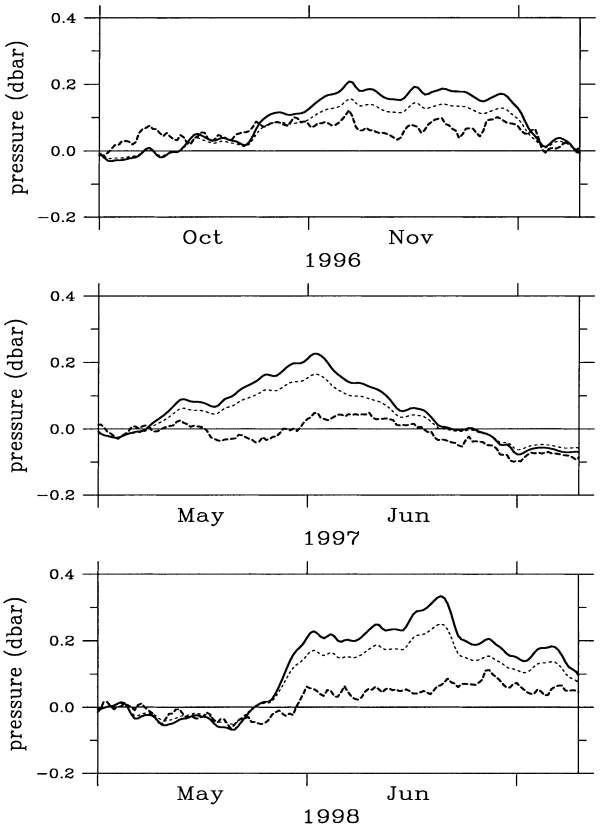

FIG. 13. Three events identified by Potemra et al. (2002) as Indian Ocean generated Kelvin waves impinging upon the Lombok Strait. In each case the solid (upper) line represents the observed pressure signal at the Bali gauge and the dashed (lower) line represents the pressure signal at the Lombok gauge (see Fig. 12b for gauge locations). The signals have been shifted to roughly line up at the beginning of each event. The dotted line represents the pressure signal one would expect at Lombok if the cross-strait decay were exponential with the Rossby radius decay scale.

For signals originating on the Pacific Ocean side, the Bali and Lombok stations span the inlet to the strait, and the situation is qualitatively different. The pressure signal at the far side of the inlet is cancelled only as total transmission is approached (cf. Figs. 12b and 12c). We would expect the Bali gauge to be insensitive to low frequency but quite sensitive to high-frequency signals originating north of Lombok Strait.

b. Nonlinear effects of throughflow and large-amplitude waves

In the linear model, a mean throughflow would simply superimpose upon the wave solution without af-

fecting it, but the throughflow in Lombok Strait can produce mean surface velocities on the order of 1 m s^{-1} (Chong et al. 2000), a sizable fraction of the Kelvin wave phase speed of $\approx$2.5 m s^{-1}. At these velocities, along-strait advection of momentum can become significant and the linear dynamics on which our model is based become less valid. A more drastic effect might arise from the amplitude of the waves themselves. The May 1997 downwelling wave observed by Sprintall et al. (2001) off the south coast of Java had surface velocities of 1 m s^{-1}, and isotherm displacements of 150 m. Assuming a sill depth and an upper layer thickness of $\sim$250 m, a downward interface displacement of this magnitude would introduce significant nonlinearity into the problem while simultaneously ensuring that a large fraction of the Kelvin wave energy will be blocked by the sill. The energy transmission will be decreased in ways that we cannot predict with the 1½-layer model. Indeed, the next strait downstream from Lombok Strait, Sumba Strait, had a response to the May 1997 wave on the same order as the Lombok Strait response (Chong et al. 2000), indicating a much smaller energy transmission for Lombok Strait than our model has predicted. The effect of a sill is in the linear limit is investigated by Wajsowicz (2002, manuscript submitted to *J. Phys. Oceanogr.*) and it is likely that a full understanding of the energy transmission characteristics of Lombok Strait will also require addressing the nonlinear effects.

7. Summary

The transmission of a subinertial linear Kelvin wave through an Ideal Strait is essentially a one-dimensional wave interference problem due to two partially reflecting features in series along the wave path. If a channel is narrow enough so that not all of the incident energy can propagate into an Entrance, then not all of the energy in the channel can propagate out of an Exit—some must be reflected back along the channel. This internal reflection within an Ideal Strait sets up the interference condition, with the important consequences that the energy transmission of a strait can be sensitive to the channel length as well as the width, and that the transmission approaches 100% at low wave frequencies.

Numerical solutions indicate that the transmission characteristics of a strait with complex coastal geometry can be well approximated by an Ideal Strait of uniform width, and that the f-plane model appears to be a good predictor for a strait on a β-plane as close to the equator as 8.5° latitude. A strait based on the 200-m contour at Lombok Strait is shown to approach near total transmission within the 30–100-day intraseasonal band.

The linear, inviscid dynamics considered here are highly idealized, as is the neglect of topographic effects, but the physics of the Ideal Strait model is so basic—in particular the reflection of Kelvin wave energy from an Exit—that the wave interference results can be expected to be robust and must be considered even when dealing with more complex dynamics and bathymetric conditions. More accurate predictions of energy transmission for the real Lombok Strait under the frequently encountered conditions of strong throughflow currents and large-amplitude waves will require the additional consideration of nonlinear and topographic effects.

Acknowledgments. The authors express their gratitude for the significant contributions to this work made by Janet Becker, Eric Firing, and Peter Müller. Specifically, the equivalence of a Kelvin wave in reverse and a Kelvin wave in the opposite hemisphere was merely a matter of physical intuition until Peter Müller noticed that the relationship was exact because of the time-reversal invariance of the governing equations. The elegant solution for the strait in the geostrophic, low-frequency limit is courtesy of Eric Firing. The mathematical insights of Janet Becker were invaluable throughout the study. Jim Potemra graciously shared the pressure gauge data presented in Fig. 13, as well as many valuable insights into the dynamics of the Indonesian region. Conversations with Rudolf Kloosterziel, Roger Lukas, and Dennis Moore also added significantly to the work, as did the stimulating comments of the two reviewers.

REFERENCES

Arief, D., and S. P. Murray, 1996: Low-frequency fluctuations in the Indonesian throughflow through Lombok Strait. *J. Geophys. Res.,* **101,** 12 455–12 464.

Buchwald, V. T., 1971: The diffraction of tides by a narrow channel. *J. Fluid Mech.,* **46,** 501–511.

——, and J. W. Miles, 1974: Kelvin-wave diffraction by a gap. *J. Aust. Math. Soc.,* **17,** 29–34.

Chong, J. C., J. Sprintall, S. Hautala, W. Morawitz, N. A. Bray, and W. Pandoe, 2000: Shallow throughflow variability in the outflow straits of Indonesia. *Geophys. Res. Lett.,* **27,** 125–128.

Griffiths, D. J., 1995: *Introduction to Quantum Mechanics.* Prentice Hall, 394 pp.

Hautala, S. L., J. Sprintall, J. T. Potemra, A. G. Ilahude, J. C. Chong, W. Pandoe, and N. Bray, 2001: Velocity structure and transport of the Indonesian throughflow in the major straits restricting flow into the Indian Ocean. *J. Geophys. Res.,* **106,** 19 527–19 546.

Killworth, P. D., 1989: Transmission of a two-layer coastal Kelvin wave over a ridge. *J. Phys. Oceanogr.,* **19,** 1131–1148.

Lighthill, J., 1978: *Waves in Fluids.* Cambridge University Press, 504 pp.

Longhurst, R. S., 1967: *Geometrical and Physical Optics.* John Wiley and Sons, 592 pp.

Longuet-Higgins, M. S., 1969: On the trapping of long-period waves round islands. *J. Fluid Mech.,* **37,** 773–784.

Miles, J. W., 1973: Tidal wave diffraction by channels and bays. *Geophys. Fluid Dyn.,* **5,** 155–171.

Molcard, R., M. Fieux, J. C. Swallow, A. G. Ilahude, and J. Banjarnahor, 1994: Low frequency variability of the currents in Indonesian Channels (Savu-Roti and Roti-Ashmore Reef). *Deep-Sea Res.,* **41,** 1643–1662.

——, ——, and A. G. Ilahude, 1996: The Indo–Pacific throughflow in the Timor Passage. *J. Geophys. Res.,* **101,** 12 411–12 420.

——, ——, and F. Syamsudin, 2001: The throughflow within Ombai Strait. *Deep-Sea Res.,* **48,** 1237–1253.

Murray, S. P., and D. Arief, 1988: Throughflow into the Indian Ocean through the Lombok Strait, January 1985–January 1986. *Nature*, **333,** 444–447.

Packham, B. A., 1969: Reflexion of Kelvin waves at the open end of a rotating semi-infinite channel. *J. Fluid Mech.*, **39,** 321–328.

Potemra, J. T., S. L. Hautala, J. Sprintall, and W. Pandoe, 2002: Interaction between the Indonesian seas and the Indian Ocean in observations and numerical models. *J. Phys. Oceanogr.*, **32,** 1838–1854.

Qiu, B., M. Mao, and Y. Kashino, 1999: Intraseasonal variability in the Indo–Pacific throughflow and the regions surrounding the Indonesian seas. *J. Phys. Oceanogr.*, **29,** 1599–1618.

Smith, W. H. F., and D. T. Sandwell, 1997: Global seafloor topography from satellite altimetry and ship depth soundings. *Science*, **277,** 1956–1962.

Sprintall, J., A. L. Gordon, R. Murtugudde, and D. Susanto, 2000: A semiannual Indian Ocean forced Kelvin wave observed in the Indonesian seas in May 1997. *J. Geophys. Res.*, **105,** 17 217–17 230.

Taylor, G. I., 1920: Tidal oscillations in gulfs and rectangular basins. *Proc. London Math. Soc.*, **20** (2), 148–181.